Transactions of the Materials Research Society of Japan 32[4] 959-962 (2007)

Investigation of the effect of microstructure on the conductivity of Sm_2O_3- and Y_2O_3-doped $BaCeO_3$ in various atmospheres

Richard Buchanan, Toshiyuki Mori and Fei Ye
Fuel Cell Materials Centre, National Institute for Materials Science, 1-1 Namiki, Tsukuba, Ibaraki, 305-0044
Fax: 81-29-860-4667, e-mail: Richard.buchanan @ nims.go.jp, (MORI.Toshiyuki @ nims.go.jp)

This work investigates the effect (if any) on the conductivities of $BaCe_{0.8}Sm_{0.2}O_{2.9}$ and $BaCe_{0.8}Y_{0.2}O_{2.9}$ at ~500°C caused by differing microstructures over a range of dry and 'wet' atmospheres. Partial oxygen pressures ranged from $1\text{-}10^{-21}$ atm. Pellets of varying microstructures were prepared using conventional sintering with heating and cooling rates of 5-80°C min^{-1} at temperatures of 1,300-1,550°C. Over the pO_2 range, the main conductivity regions observed are a p-type contribution at $1\text{-}10^{-4}$ atm and an n-type contribution at 10^{-18}-10^{-21} atm. The relationship between conductivity and microstructure in different atmospheres for BaCeY20 and BaCeSm20 can be slightly complicated. Generally, for BaCeY20, conductivity appears to increase with increasing heating rate or grain size up to a maximum (~15-20°C min^{-1} or ~720-803nm), then decreases after that. For $BaCe_{0.8}Sm_{0.2}O_{2.9}$ it is more difficult, as conductivity/ grain size or heating rate trends varying from atmosphere to atmosphere.

Key words: conductivity, doped $BaCeO_3$, pO_2, proton-conductor.

1: INTRODUCTION

The discovery of proton conduction in doped $SrCeO_3$ in 1981 [1] sparked interest in potential proton-conducting electrolyte materials. Later, doped $BaCeO_3$ [2, 3] was discovered to have proton conductivity as well and is supposed to have the best proton conductivity out of the perovskite proton-conductors $BaCeO_3$, $BaZrO_3$, $SrCeO_3$ and $SrZrO_3$ [3].

These materials have drawbacks, however, as they react with CO_2 [4, 5]. High temperatures of up to or exceeding 1,600°C are required for reaction and sintering. At these temperatures, the stoichiometry can change, due to the possibility of BaO volatilization [6, 7]. Thermodynamic studies have shown that there can be a Ba vapour pressure of around 10^{-5} atm at ~1,600°C [8].

Preparation of single-phase oxides using solid-state reaction requires temperatures of 1,250-1,500°C, along with sintering temperatures of 1,500-1,675°C to prepare dense pellets [3, 9]. Preparation methods such as the Pechini process [5, 10] and oxalate co-precipitation [11, 12] have been used to try and reduce these temperatures. Success has been limited, as calcination temperatures were reduced but sintering still requires temperatures of at least 1,450°C.

Some progress has been made using alternative preparation methods. One example involved the preparation of $BaCe_{0.8}Sm_{0.2}O_{2.9}$ using an auto-ignition method. The resultant powders could be calcined at ~850°C, yielding the desired oxide and a small $BaCO_3$ impurity that disappears upon sintering. Pellets prepared using these powders could be sintered to 99% density at 1,300°C [13].

The main question asked in this work is whether microstructures of sintered pellets affect the conductivities of $BaCe_{0.8}Y_{0.2}O_{2.9}$ (BaCeY20) or $BaCe_{0.8}Sm_{0.2}O_{2.9}$ (BaCeSm20) in a range of dry and humid atmospheres over a pO_2 range of 10^{-21}-1 atm.

2: EXPERIMENTAL

2.1: Precursor Preparation

Compositions used in this work were $BaCe_{0.8}Y_{0.2}O_{2.9}$ (BaCeY20) and $BaCe_{0.8}Sm_{0.2}O_{2.9}$ (BaCeSm20). Reagents used were $Ba(NO_3)_2$ (99.999%, Aldrich), $Ce(NO_3)_3.6H_2O$ (99.99%, Kantō Chemical Company), $Y(NO_3)_3.6H_2O$ (Kantō, 99.99%), $Sm(NO_3)_3.6H_2O$ (99.95%, Kantō), NH_4HCO_3 (Kantō, ≥96%) and $(NH_4)_2CO_3$.(Wakō Pure Chemicals, ≥30% as NH_3) All chemicals were used as received.

Mixed nitrate solutions were prepared by dissolving mixtures of metal nitrates in the correct stoichiometric ratios into 300ml of distilled water (total cation concentration of 0.15-0.30M). Dissolution was aided by mild stirring at room temperature or 40° for ~30 minutes. The precipitant ($(NH_4)_2CO_3$ or NH_4HCO_3, 0.5-3M) was dissolved in 300 or 450ml of distilled water at the reaction temperature (room temperature, 50°C or 70°C). In the co-precipitation reaction, the mixed nitrate solution was added drop wise (1-2 drops/ second) to the precipitant solution that was maintained at the reaction temperature throughout the precipitation, with gentle stirring. After adding all of the mixed nitrate solution, the reaction mixture was allowed to develop for 1-24 hours at the reaction temperature with gentle stirring. Generally, the reaction mixture was white, apart from a few cases where the colour was more pale yellow.

Next, the mixture was filtered by suction filtration and washed three times with water and once with ethanol, with filtration after each washing. After the final filtration, the precipitate was blow-dried with flowing nitrogen at room temperature for at least 48 hours. Then, the dried product was crushed in an alumina mortar and pestle and sieved. Finally, powders were calcined at temperatures of between 850-1,000°C for at least 4 hours in oxygen (~300cm^3 min^{-1}), to provide a range of powders suitable for sintering at different temperatures.

2.2: Pellet Preparation and Sintering

Firstly, pellets were pressed uniaxially at ~20 MPa, followed by cold isostatic pressing for 5 minutes at 200-240 MPa. For general sintering, pellets were heated at 5°C min^{-1} to temperatures between 1,300 and 1,550°C, holding for 6-8 hours. Sintered densities were determined using the Archimedes method and pellets can be sintered to at 95-100% density over this temperature range.

For heating rate dependence work, pellets of BaCeY20 were sintered at 1,450°C and pellets of BaCeSm20 were sintered at 1,400°C at various heating rates of 5-80°C min^{-1}, followed by an isothermal hold for 6 hours, then cooling at 5-80°C min^{-1} in a Setaram TMA 92-1750 Thermomechanical Analyser, which was used purely as another sintering furnace. Pellets were covered in platinum foil to prevent contamination of the instrument.

2.3: SEM Observation

Hitachi S-4800 and S-5000 scanning electron microscopes were used to examine the sizes of grains and the microstructures of sintered pellets.

The pellets were polished with a diamond paste to a 1μm mirror finish. This was followed by thermal etching, where pellets were heated at 100°C below the original sintering temperature for 2 hours. Finally, the pellets were coated with platinum. Average grain sizes for sintered pellets were determined using the average linear intercept method, observing at least 250-300 grains per sample [14]. Grain sizes for sintered pellets ranged from 702-1,740nm for BaCeSm20 and 496-1,108nm for BaCeY20.

2.4: Conductivity Measurements

Three-terminal DC conductivity measurements were carried out over a pO_2 range of $0.2\text{-}10^{-21}$ atm. Samples were circular pellets 10-13 mm in diameter and 1-2 mm thick, with platinum electrodes painted on both circular faces and fired in air at 1,000°C for 1-2 hours.

The atmospheres used were as follows (pO_2 levels are shown in parentheses): oxygen (0.9-1 atm), air (0.1-0.2 atm), argon (~10^{-3} atm), 'wet' argon (10^{-2}-10^{-3} atm), 10% H_2/ He (10^{-20}-10^{-21} atm) and 'wet' 10% H_2/ He (~10^{-19} atm). pO_2 levels were measured using an external oxygen sensor operating at 800°C that monitored the outlet gases, with the e.m.f. measured by a voltmeter and the pO_2 was calculated using the Nernst equation, shown as equation 1.

$$pO_2 \text{ (measured)} = 0.209 \exp(-4VF/RT) \quad \{1\}$$

'Wet' atmospheres were provided by bubbling the appropriate gas through water. Gas flow rates used were ~200 cm^3 min^{-1} for dry argon and oxygen, 100 cm^3 min^{-1} for 'wet' argon and 50 cm^3 min^{-1} for 'wet' and dry 10% H_2/ He.

Conductivities were measured with the furnace holding isothermally at ~570°C throughout. In air, oxygen and argon ('wet' and dry), sample temperatures were 500±4°C. In 'wet' and dry 10% H_2/He, sample temperatures were 515±5°C, due to thermal conductivity differences between H_2/He and air/ argon/ oxygen atmospheres. Duplicate measurements were taken for each atmosphere, except for air, with the samples allowed to equilibrate for at least 15-30 minutes before measurement.

3: RESULTS AND DISCUSSION

3.1: BaCeY20

Figure 1 shows an example plot of how the conductivity of BaCeY20 changes with pO_2. The main components seem to be a p-type electronic contribution at higher pO_2 and a smaller n-type electronic contribution at low pO_2. The slopes observed in these regions usually vary between 1/4 and 1/6, with some slopes being less steep (1/8 or lower).

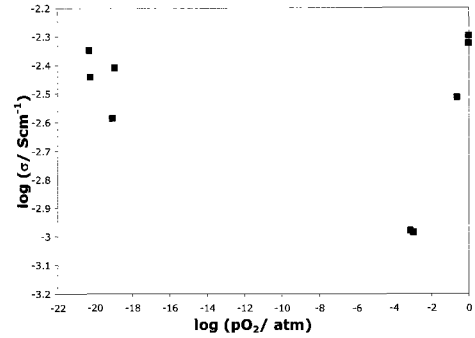

Figure 1: Conductivity/ pO_2 plot for BaCeY20

The relationship between conductivity with pellet grain size for each atmosphere is a simple trend, mixed in with a more complex region.

In all atmospheres apart from oxygen, it appears that conductivity increases with grain size increasing from 496 nm to a maximum at 702-803 nm, then conductivity decreases with increasing grain size after that. An example of this is shown in Figure 2. In oxygen, the conductivity trends are inverted.

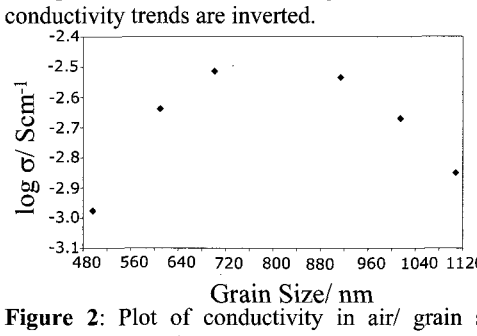

Figure 2: Plot of conductivity in air/ grain size for BaCeY20 sintered at 1,310-1,550 °C

In the case of the conductivity/ grain size dependence, the trends suggest that in the lower grain size region, the conductivity is influenced by space charge layers. The space charge layer model suggests that there is a segregation of dopant cations and a resultant oxygen vacancy reduction around grain boundaries, leading to the formation of space charge layers. When grain size is decreasing, this leads to an increase in grain boundary density that makes this effect more significant and reducing total conductivity [15]. When grain size increases in this region, this influence of this effect diminishes.

In the higher grain size region, where the conductivity decreases with increasing grain size, this is likely to be due to the formation of 'domains'. 'Domains' form when some of the oxygen vacancies introduced by yttrium

doping associate with each other to form clusters which do not participate in conductivity. As a result, with increasing grain size, the tendency towards cluster formation increases and conductivity decreases.

The relationship between conductivity and heating rate is similar (based on a group of pellets sintered at 1,440-1,450°C) and may be due to similar factors.

For this group of pellets heated at rates ranging from 5-80°C min^{-1} and cooled at 5°C min^{-1}, conductivity increased with increasing heating rate to a maximum, then decreased after that. The conductivity maxima were at 10°C min^{-1} for air, 15°C min^{-1} in argon and oxygen and at 20°C min^{-1} for 'wet' and dry 10% H_2/ He. This is shown in Figure 3.

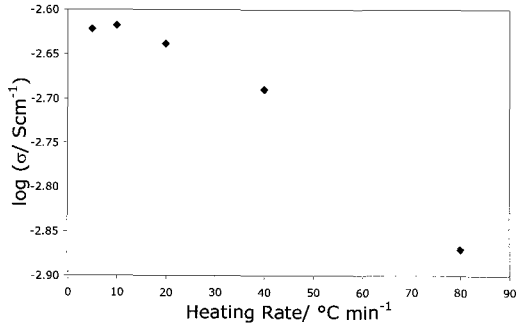

Figure 3: Conductivity in air/ heating rate relationship of BaCeY20 (Heating rates 5-80°C min^{-1}, cooling rate 5°C min^{-1})

In the case of pellets heated at 5-80°C min^{-1} and cooled at the same rate, the trends were similar, as shown in Figure 4. In air, oxygen and dry 10% H_2/ He, conductivity increased with increasing heating rate up to 20°C min^{-1}. In argon, the opposite trend happened, where conductivity decreased with heating rate increasing to a minimum at 20°C min^{-1} and increased after that. In 'wet' 10% H_2/ He, however, conductivity alternated between increasing and decreasing with heating rate.

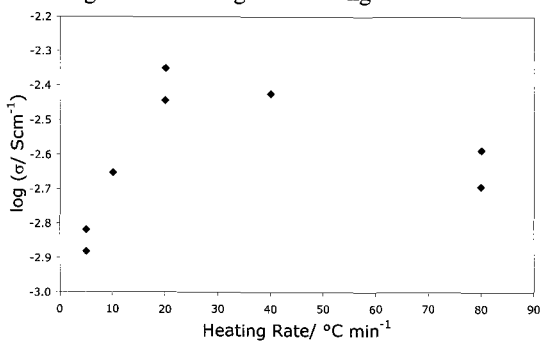

Figure 4: Conductivity/ heating rate relationship of BaCeY20 (Heating rates 5-80°C min^{-1}, with identical cooling rates)

3.2: BaCeSm20

The way in which the conductivity of BaCeSm20 changes with pO_2 is similar to that of BaCeY20, as shown in Figure 5.

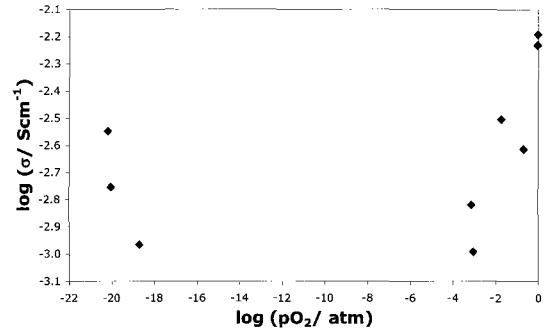

Figure 5: Conductivity/ pO_2 plot for BaCeSm20

The relationship between conductivity and pellet grain size over the pO_2 range is not simple, and there does not seem to be a trend that is common to all atmospheres.

In air, the trend appears to be for conductivity to increase initially with grain size, then decrease after a maximum at 943nm. In oxygen and argon, conductivity generally increases with increasing grain size but in 10% H_2/ He, conductivity appears to decrease with increasing grain size to 1,216 nm, possibly starting to increase with increasing grain size after that. In 'wet' 10% H_2/ He, there are occasions of conductivity increasing or decreasing with increasing grain size. Finally, in 'wet' argon, the trend is slightly similar to that of dry 10% H_2/ He. Thus, the conductivity/ grain size relationships differ somewhat with atmosphere.

In terms of conductivity/ heating rate dependence, there is no common trend between conductivity and heating rate shared by all atmospheres. In air, it is implied that the conductivity either rises or decreases slightly with increasing heating rate up to 40°C min^{-1}, then decreases slightly at 80°C min^{-1}. In oxygen, the main trend is similar, but to a smaller extent and there are also other samples that show at 5 and 10°C min^{-1}, decreasing conductivity with increasing heating rate.

In argon and dry 10% H_2/ He, the trend alternates between conductivity increasing and decreasing with increasing heating rate. In 'wet' 10% H_2/ He, after an initial rise, conductivity seems to decrease with increasing heating rate from 10°C min^{-1}. Finally, in 'wet' argon, conductivity generally increases with increasing heating rate.

Overall, it can be said that while there is general agreement with the direction of conductivity with grain size or heating rate for BaCeY20, the same cannot be said for BaCeSm20, where the trends are more complex and varied, where it shows one tendency in some atmospheres and different tendencies in the others.

For BaCeY20, the trends appear to be that conductivity increases with increasing grain size or heating rate up to a maximum, then decreasing after that.

For BaCeSm20, the conductivity/ grain size relationship is complex, varying with atmosphere. The heating rate dependence also varies with atmosphere, but it appears to be simpler. In air and oxygen, the relationship is similar to that found in BaCeY20 but inverts in 'wet' 10% H_2/ He. In argon and dry 10% H_2/ He, it alternates and in 'wet' argon, the trend is simplest, where conductivity increases with increasing heating rate.

Perhaps additional forms of micro or nano-structure analysis would be helpful in determining if there are any

other microstructural features that could be involved.

4: CONCLUSIONS

The conductivity/ pO_2 dependences between BaCeY20 and BaCeSm20 show similar behaviour, with a p-type electronic contribution at high pO_2 and a smaller n-type electronic contribution at low pO_2.

The relationship between conductivity and microstructure in different atmospheres for BaCeY20 and BaCeSm20 can be slightly complicated. Generally, for BaCeY20, conductivity appears to increase with increasing heating rate or grain size up to a maximum, then decreases after that. For BaCeSm20, however, it is more difficult, with conductivity/ grain size or heating rate trends varying from atmosphere to atmosphere. Perhaps additional forms of microstructural analysis could shed more light on the conducting properties of these materials.

REFERENCES

[1] H. Iwahara, T. Esaka, H. Uchida, N. Maeda, Solid State Ionics, **3/4**, 359-363 (1981)
[2] A. Mitsui, M. Miyayama, H. Yanagida, Proceedings of the 3rd Meeting on Chemical Sensors, pgs 43-, Tōkyō, Japan (1984)
[3] H. Iwahara, H. Uchida, K. Ono, K. Ogaki, Journal of the Electrochemical Society, **135** (2), 529-532 (1988)
[4] H. Uchida, A. Yasuda, H. Iwahara, Denki Kagaku, **57**, 153- (1989)
[5] M.J. Scholten, J. Schoonman, J.C. van Miltenburg, H.A.J. Oonk, Solid State Ionics, **61**, 83-91 (1993)
[6] D. Shima, S.M. Haile, Solid State Ionics, **97**, 443-455 (1997)
[7] S.M. Haile, G. Staneff, K.H. Ryu, Journal of Materials Science, **36**, 1149-1160 (2001)
[8] R. Saha, R. Babu, K. Nagarajan, C.K. Matthews, Thermochimica Acta, **120**, 29- (1987)
[9] A. Tomita, T. Hibino, M. Suzuki, M. Sano, Journal of Materials Science, **39**, 2493-2497 (2004)
[10] V. Agarwal, M. Liu, Journal of the Electrochemical Society, **143** (10), 3239- (1996)
[11] S.D. Flint, R.C.T. Slade, Solid State Ionics, **77**, 15- (1995)
[12] F. Chen, O.T. Sorensen, G. Meng, D. Peng, Solid State Ionics, **100**, 63- (1997)
[13] A. Chakroborty, A. Das Sharma, B. Maiti, H.S. Maiti, Materials Letters, **57**, 862-867 (2002)
[14] M.I. Mendelson, Journal of The American Ceramic Society, **52** (8), 443-450 (1969)
[15] X. Guo, Solid State Ionics **81**, 235-242

ACKNOWLEDGMENT

Funding for this work was provided by Japan Society for the Promotion of Science.

(Received January 5, 2007;Accepted Sepember 1, 2007)